Microelectronic Engineering 262 (2022) 111834

Contents lists available at ScienceDirect

Microelectronic Engineering

journal homepage: www.elsevier.com/locate/mee

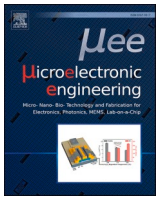

Synthesis and analysis of TiO_2 nanotubes by electrochemical anodization and machine learning method for hydrogen sensors

Esme Isik [a], Lutfi Bilal Tasyurek [a], Ibrahim Isik [b,*], Necmettin Kilinc [c]

[a] Department of Optician, Malatya Turgut Özal University, 44210 Malatya, Turkey
[b] Department of Electrical Electronics Engineering, Faculty of Engineering, Inonu University, 44280 Malatya, Turkey
[c] Department of Physics, Faculty of Science & Arts, Inonu University, 44280 Malatya, Turkey

ARTICLE INFO

Keywords:
Titanium dioxide
Nanotubes
Hydrogen sensor
Anodization
Support vector machine
Artificial neural network

ABSTRACT

The conductometric hydrogen gas sensors were used to explore TiO_2 nanotubes in this study. TiO_2 nanotubes are synthesized by anodization of the titanium foils using a neutral 0.5% and 1% (wt) NH_4F in glycerol solution depending on anodization time and anodization voltage at the temperature of 20 °C. The amorphous, rutile and anatase phases of TiO_2 are observed for as-prepared TiO_2 nanotubes, annealed at 700 and 300 °C, respectively. The diameters of the nanotubes grow as the anodization time and voltage increase, according to scanning electron microscopy (SEM) images. The inner diameter of nanotubes is changed between ~70 nm to ~225 nm. Hydrogen sensing properties of Ti/TiO_2 nanotubes/Pd device has been tested at room temperature under concertation range from 0.5% to 10% depending on the crystalline phase. The highest sensor response is observed for anatase crystalline TiO_2 nanotubes. Typical Schottky-type behavior is observed from the I-V measurement. All the fabricated nanotube diameters are also simulated by using Support Vector Machine and Artificial Neural Network models. And also, some of the nanotube diameters which are not obtained experimentally (anodization voltage of 70 V) are estimated using the Support Vector Machine and Artificial Neural Network models. In addition, an analytical model is also proposed using Jacobi numeric analysis method alternative to the simulation model for the nanotube diameter. Finally, the analytical, simulation, and experimental results are compared, and the best result is obtained using the 1 Hidden Layer Artificial Neural Network model.

1. Introduction

As an environmentally friendly, useful, cost-effective clean fuel, hydrogen attracts attention among sustainable energy sources [1]. Therefore, it has many industrial uses such as engines of rocket, fuel cell technology and applications of automotive [2]. When hydrogen is coupled with oxygen, however, it becomes exceedingly volatile, flammable, and explosive. It has a dangerous structure that can easily ignite when the hydrogen concentration is >4% in the air [3]. For this reason, highly sensitive, fast and selective H_2 detection sensors are required to monitor the H_2 concentration. Catalytic, electrochemical, thermal conductivity, work-function-based, resistance-based, mechanical, acoustic and optical techniques are all used in hydrogen detection technologies [4].

Due to their remarkable features, such as chemical stability [5], biocompatibility [6], high photocatalytic activity [7], and efficacy in terms of dye-sensitized solar cells, cost semiconductors, catalysis, water treatment, and gas sensors are just a few of the applications for TiO_2 materials [8]. Rutile [9], anatase [10], and brookite [11] are three natural polymorphs of TiO_2, each with its own set of characteristics. Sol–gel, hydrothermal, chemical vapor deposition, and solvothermal preparation techniques can be used to produce TiO_2 into a variety of nanostructures, including nanorods, nanoparticles, nanotubes, nanowires, and mesoporous/nanoporous materials [12,13]. Depending on the application, each approach offers advantages and disadvantages. Nanotubes are fascinating because of their high surface-to-volume ratio and size-dependent properties. Nanotubes are suitable for gas sensors since they have a huge surface area and are one-dimensional [14]. After the regular synthesis of TiO_2 nanotubes arrays by Grimes et al. [15], researches were made for their effects on many applications such as solar cells [16,17], photocatalysis [18], chemical sensing [19], drug delivery applications [20] and gas sensor [21]. The ability to adjust parameters such as tube length and diameter [22] has enabled gas detection to work at both low temperatures and ppm levels [23]. For

* Corresponding author.
E-mail address: ibrahim.isik@inonu.edu.tr (I. Isik).

https://doi.org/10.1016/j.mee.2022.111834
Received 4 April 2022; Received in revised form 10 June 2022; Accepted 18 June 2022
Available online 25 June 2022

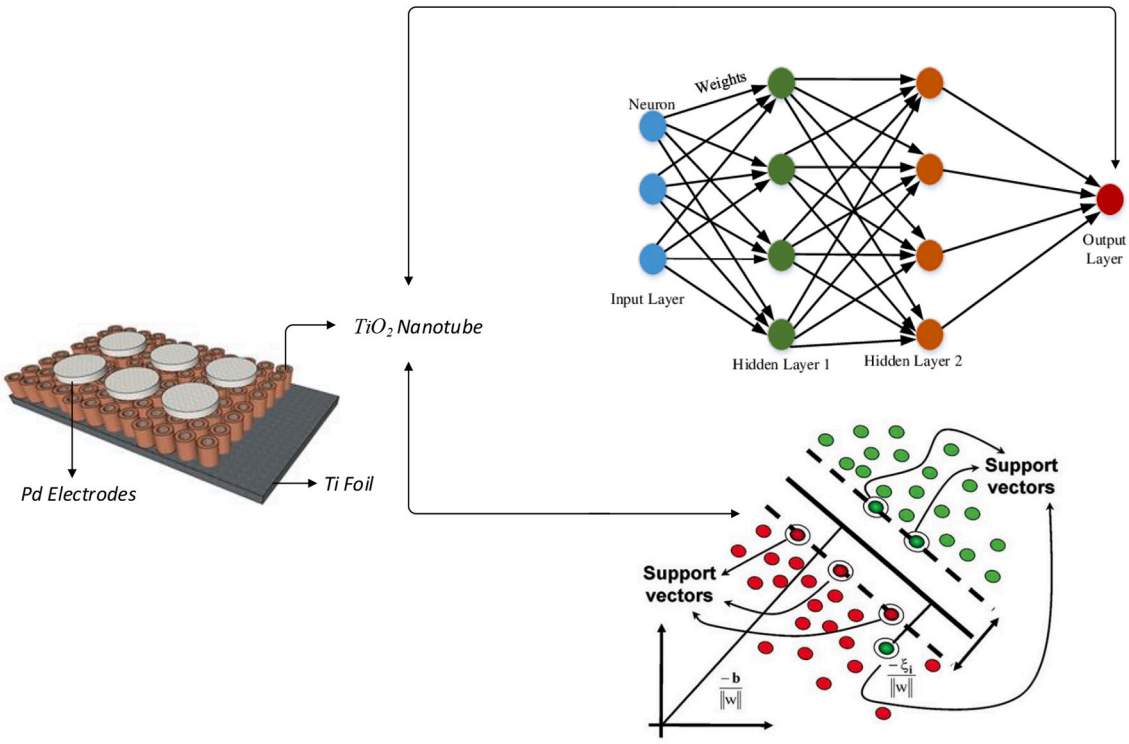

Fig. 1. Schematic diagram of the as-growth gas sensor with SVM and ANN models.

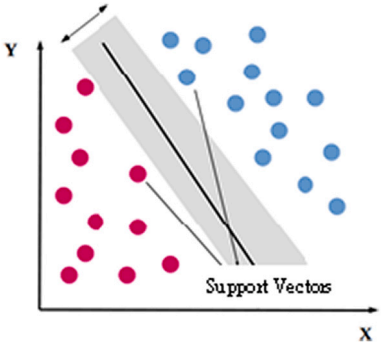

Fig. 2. SVM schematic representation.

safety and industrial health, automotive applications, environmental monitoring, and manufacturing process management, gas sensors are becoming increasingly vital.

Zwilling et al. originally described electrochemical anodization of TiO_2 nanotubes to get a highly ordered structure using a chromic acid–hydrofluoric acid (HF) combination solution. [24] and Gong et al. used HF electrolytes to produce TiO_2 nanotubes [15] Beranek et al. also used an H_2SO_4–HF combination solution as well [25]. In addition to these solutions, TiO_2 nanotubes continued to be produced by researchers using many different solutions. The production of TiO_2 nanotubes using a glycerol-based electrode and its effect in various applications have attracted attention. Macak et al. were the first to report that a glycerol solution could be used to produce self-organizing TiO_2 nanotubes having a large aspect ratio. Especially since the effect of TiO_2 nanotube arrays on H_2 gas is remarkable, the glycerol-based electrolyte was preferred. The architecture of the TiO_2 nanotube arrays generated by anodizing the Ti foil in a glycerol-based electrolyte containing fluorine ions resulted in considerable resistance variation. [26].

In the last few years, the effects of TiO_2 nanotubes synthesized using various methods on the selectivity, response time, sensitivity, etc.

Table 1
System parameters of the proposed ANN and SVM models.

Network type	Feed forward back propagation algorithm
Transfer function	Tansig
Initialization of the weights	Sigmoid
Training function	Trainlm
Adaptation learning function	Learngdm
Performance function	MSE
Number of layers	1 and 2
Optimization procedure	Levenberg-Marquardt

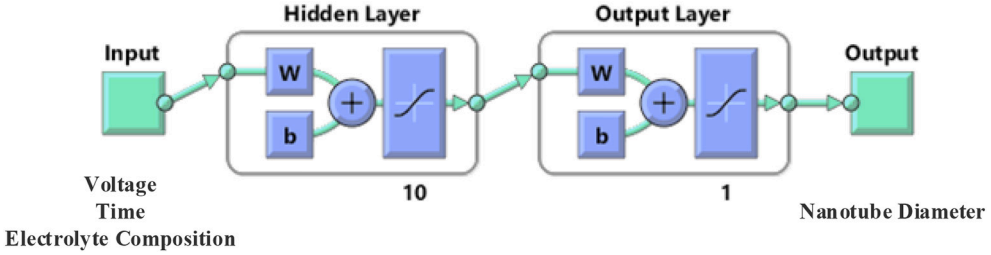

Fig. 3. The proposed ANN model with input, output and hidden layer.

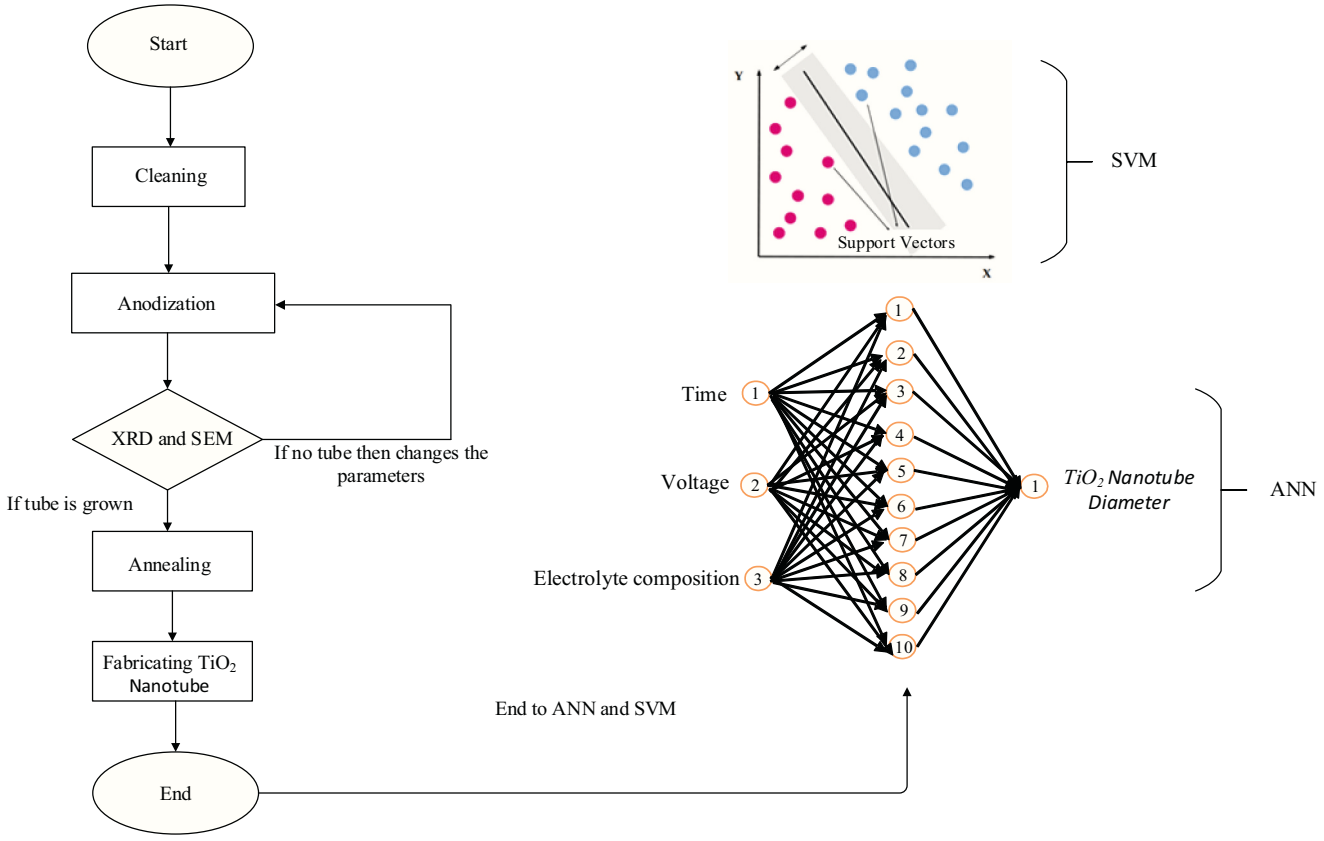

Fig. 4. Flow chart of the fabrication, simulation and prediction of the TiO_2 nanotubes with ANN and SVM models.

parameters of H_2 gas have been investigated. In researches on H_2 sensor applications of TiO_2 nanotubes arrays are used for different anodization methods such as 0.5% HF [27], 1 wt% HF [28], NH_4F in ethylene glycol (EG) [29], $(NH_4)_2SO_4$ and 0.5 wt% NH_4F [30], glycerol solution containing NH_4F [31], glycerol containing $(NH_4)_2SO_4$ and NH_4F [32]. There are also variable pH values for the electrolytes sodium hydrogen sulfate ($NaHSO_4$) monohydrate, potassium fluoride (KF) and sodium citrate tribasic dehydrate. [26]. By combining a template aided technique with atomic layer deposition, anodic aluminum oxide (AAO) was employed to create TiO_2 nanotubes (ALD) [33]. Besides, H_2 gas sensitivity was also investigated using TiO_2 nanotubes produced by the the hydrothermal synthesis method [34]. Pt, Pd, Au, Ag and Cu electrodes, Au, Ag and Pt wire bonders [35] and Pd nanorings [36] were used to take current-voltage (I-V) measurements. In these studies, the researchers investigated the sensing properties against H_2 flow at concentrations ranging from 0.5% to 10%.

There are also some simulation based TiO_2 nanotubes studies in the literature [37]. The distribution, diameter and length of the TiO_2 nanotubes prepared by anodization (acidic HF mixtures, water free, buffered neutral or HF electrolytes) is predicted by using the artificial neural network (ANN) model with back propagation method [38]. The choice of training data, in addition to the construction and limits of the networks, are examined in this model. The R value of training and testing data was 0.9806 and 0.9997, separately, and the percentage of significant nanotube spreading estimate values was 93.48%. The testing data had a relation difference of 4.5%, and the predictive value of the generated network was claimed to be perfect enough to be employed in further nanotube length modeling studies [38]. There are many learning algorithm methods, such as active learning in literature developed using machine learning (ML) [37]. Bipolar electrochemistry is utilized to assist the optimization process of generating TiO_2 nanotubes micro-patterns (TNMs) with an extensive length range inside one model utilizing the active learning method. To assess or classify the training data pattern, prediction models are created using ML (Machine Learning) approaches. The gradient boosted regression tree (GBRT) model is employed in this suggested study to predict and optimize TNMs. As a result, the least experiment can enlarge the diameter range of TNMs. Bayes, K-Nearest Neighbor (KNN), Support Vector Machine (SVM), Gradient Boosting Decision Tree and Decision tree (DT) are among the classification techniques tested to distinguish cut-off points from the standard dataset (GBDT). Both the DT and GBDT approaches are found to be more accurate than other methods, with the GBRT model's R^2 value being 0.78 [39].

In the publications reported here, TiO_2 nanotubes were produced by various anodization methods. These studies generally examined some of the anodization parameters in the production of TiO_2 nanotubes. In our study, contrary to the literature, the effects of anodization parameters such as anodization temperature, voltage, time and electrolyte concentration were examined together comparatively. All parameters were evaluated more comprehensively and compared with analytical and simulation models. In this study, anodic oxidation method was used by preparing various glycerol solutions to produce TiO_2 nanotubes. Thus, the effects of anodization parameters such as anodization temperature, time, voltage, and NH_4F ratio on TiO_2 nanotube diameters were investigated. After anodizing, TiO_2 nanotubes were annealed at 300 °C and 700 °C to see the effect of crystal structures on H_2 gas sensing measurement. Thus, the effects of rutile, amorphous, and anatase crystal structures were investigated. Palladium (Pd) electrodes are coated in order to make TiO_2 nanotube gas sensor measurements produced with glycerol solutions at different ratios. TiO_2 nanotubes were tested and analyzed as a hydrogen sensor using the conductometric-based sensing method. Finally, after the diameters of all produced nanotubes are obtained, a simulation based ANN and SVM models and analytical based Jacobi method are used to obtain same results which are obtained

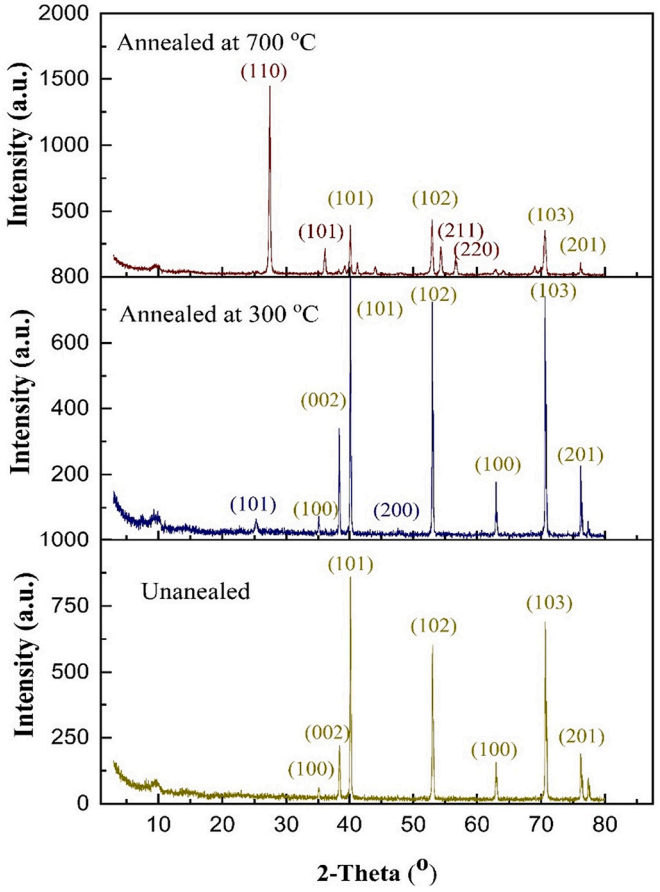

Fig. 5. XRD pattern of (a) as-anodized TiO_2 nanotubes, (b) TiO_2 nanotubes annealed at 300 °C for 3 h and (c) TiO_2 nanotubes annealed at 700 °C for 3 h.

experimentally. Thus, it will be possible to simulate and predict some unknown values of TiO_2 nanotube diameters using proposed simulation and analytical based models. As a result, all experimental, analytical and simulation results were compared.

2. Experimental and simulation procedure

2.1. Synthesis of TiO_2 nanotubes

High quality titanium foils (99.7%, Sigma-Aldrich) have a thickness of 0.25 and an area of 10 × 20 mm^2 used to growth TiO_2 nanotubes. Titanium foils were cleaned with ultrasonic treatments in deionized (DI) water, isopropyl alcohol, and acetone for 15 min prior to electrochemical anodization. The solutions of electrolyte are made from 99.5% wt glycerol and 0.5 and 1% wt NH_4F, respectively, at 20 °C. At room temperature, the electrolyte is mixed with a magnetic stirrer, and then the temperature of the electrolyte is set to 20 °C using a thermostat bath. A two-electrode system (2-cm separation) is employed in the anodization process, using a DC power source and platinum foil (99.9%, Sigma-Aldrich) as the cathode. At the anodization process, voltage is changed from 20 V to 60 V with an anodization time of 60 min to 240 min. After anodization, the samples are rinsed with DI water and dried with a high purity nitrogen gas. X-ray diffraction (XRD, Rigaku RAD-B) with Cu K radiation is used to characterize the produced TiO_2 nanotubes. Scanning electron microscopy is utilized to examine the nanotubes' morphologies and microstructure (SEM, Leo-EVO 40).

2.2. Sensor test

In order to perform gas sensing measurement, the nanotubes are annealed at 300 and 700 °C with a heating rate of 2 °C/min under dry air flow by using a tube furnace (Protherm) for 3 h. Palladium (Pd) electrodes are coated on the annealed and unannealed TiO_2 nanotubes by using a sputtering system (Nanovak 400) by using a shadow mask. The rate of deposition is remained fixed as 1 Å/s under 5 mTorr argon (Ar) pressure during the process of deposition, and the thicknesses of Pd electrodes are recorded as 120 nm by using a QCM from Inficon. In order to compute two point electrical measurements, TiO_2 nanotubes with Pd electrodes on top are contacted as a upper electrode and Ti was contacted as a bottom electrode for H_2 gas sensing measurements for obtaining Pd/ TiO_2 nanotubes/Ti structure. All measurements are done at room temperature. The fabricated nanotubes sensors are exposed to 10% H_2 after cleaning dry air to the measurement cell for the I-V characterization. The measurement system includes the mass flow control unit, a source measure unit, gas cylinders and a measurement cell with a11 volume. To change the concentration of H_2, dry air-H_2 mixtures are used. The total flow rate of the gas mixtures is adjusted to 200 sccm using two digital mass flow controllers [40]. The concentration of H_2 is changed from 0.5 to 10%. The Labview program was used to record all measurement data, which was connected to a personal computer via a GPIB data acquisition system. Fig. 1 illustrates a schematic design of the as-growth gas sensor.

2.3. ANN and SVM models

The ANN and SVM models are used for the analysis and estimation of the TiO_2 nanotubes diameter using the experimental data of time, voltage and electrolyte composition in this present study. The projected models are used with three stages. Firstly, data set were generated by classification the items automatically with time, voltage and electrolyte composition class labels according to the nanotube diameters that obtained experimentally. Secondly, the data was pre-processed and normalized. Lastly, SVM and ANN models that are developed in Matlab 2020b were trained using the nanotube diameter features. The suggested ML-based models' operation was measured utilizing the determination coefficient (R^2) and Root Mean Squared Error (RMSE) approaches. RMSE and R^2 metrics can be evaluated as follows.

$$RMSE = \sqrt{\frac{\sum_i (Exp_i - Sim_i)^2}{N}}, \quad (1)$$

$$R^2 = 1 - \frac{\sum_i (Exp_i - Sim_i)^2}{\sum_i (Sim_i)^2}, \quad (2)$$

where Sim, Exp, and N are the values of simulated and experimental findings, and the number of examples in the suggested model.

2.3.1. Support Vector Machine (SVM)

SVM stands for supervised learning model with related learning algorithms for classification and regression analyses in machine learning. SVM is a strong machine learning technique that may be broken down into linear and non-linear lines utilizing Vapnik's statistical learning model [41]. This model is a classification approach based on supervised learning tiny data and may be utilized for classification and regression analyses [42]. SVM starts by transferring the input data to a higher-dimensional space where two groups may be divided by a hyperplane that enlarges the margin between them [43]. The more space between the two classes in SVM, the more accurate the classification. Fig. 2 shows the SVM that divides the two classes on the ideal hyper plane. There are many models of SVM in literature such as linear, quadratic, cubic and medium gaussian. In this study, linear and quadratic SVM models are

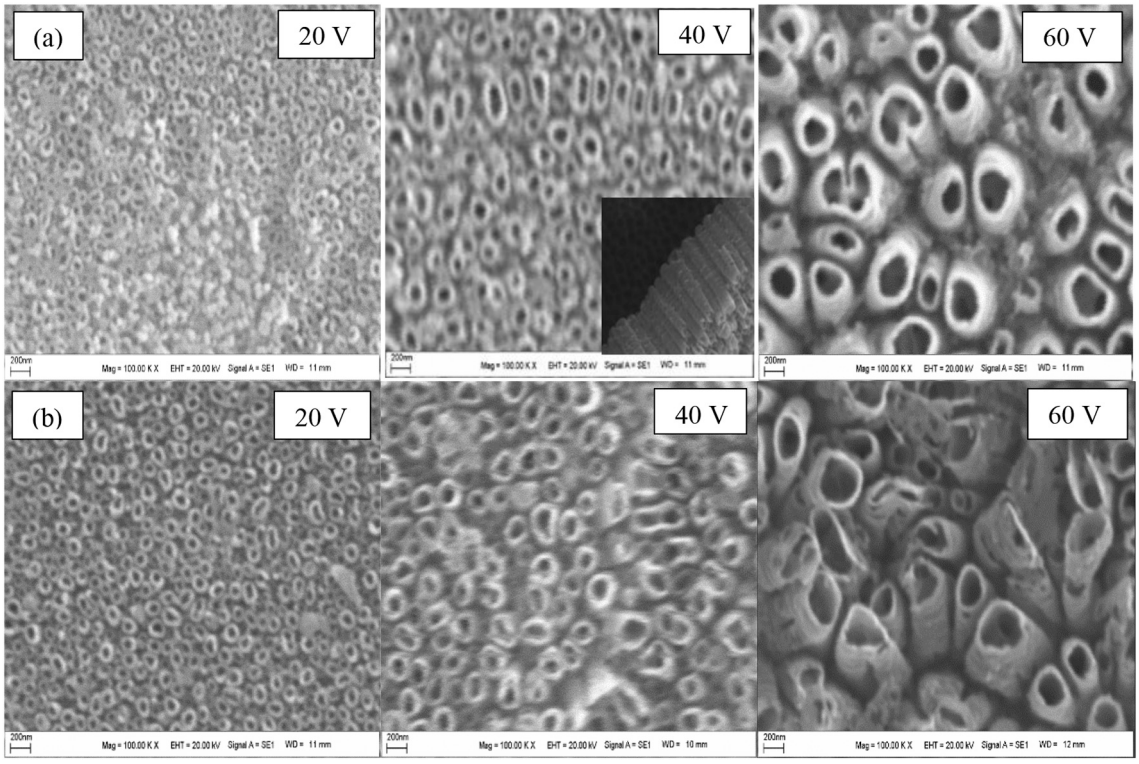

Fig. 6. Top view SEM images of TiO_2 nanotubes at the same magnification (×100,000) synthesized by applying anodization voltage from 20 V to 60 V at electrolyte composition of (**a**) 0.5% wt NH_4F, (**b**) 1% wt NH_4F.

used because of low RMSE values between output and target data. SVM model is trained using Radial Basis Function and Polynomial kernels.

SVM utilize a restricted quadratic optimization difficulty grounded on essential risk minimalize to generate the best hyperplane $f(x) = 0$ through data sets [44].

Input vectors are $\{x_i, i = 1, \ldots, n\}$ and $y_i\{-1,1\}$ fits to one of two periods, the hyperplane may be shown as:

$$w_0.x + b_0 = 0 \tag{3}$$

where w, x and b shows weight, input and bias vectors, respectively. The data may be separated linearly in the following formulas with known w and b:

$$w.x_i + b \geq 1 \; if \; y_i = 1 \tag{4}$$

$$w.x_i + b \leq 1 \; if \; y_i = -1 \tag{5}$$

It is known that the kernel method is utilized to resolve a nonlinear case by a linear classifier. The function converts the input data into a upper-dimensional characteristic space Φ. K kernel function:

$$k(x, x') = (\Phi(x), \Phi(x')) \tag{6}$$

- Polynomial

$$k(x_i, x_j) = (x_i.x_j + 1)^d \tag{7}$$

- Radial Basis Function

$$(x, y) = e^{-\gamma \|(x - x_i\|^2} \tag{8}$$

2.3.2. Artificial Neural Network (ANN)

The artificial neural network (ANN) is a data processing technique stimulated by the human brain. Currently, researchers have been used ANN to simulate and estimate their experimental results in various fields of science and engineering, containing chemistry and physics moslty [45–49]. ANN is a mathematically based model having input, output, and a layer of neurons. As illustrated in Fig. 3 [50,51], these neurons are connected in a network formation with some numerical values called weights in order to identify interactions between output and input data and finally find the closest simulation and prediction outcomes of the output data. Each weight have a particular rate which is accepted across the network and reproduced by the samples [50,51].

The system model of ANN has three inputs with 30 samples (3*30), one and two hidden layers each with ten neurons, and one output with 30 samples (1*30) based on experimental data. As shown in Fig. 3, the system model's inputs are voltage, time, and electrolyte composition, while the output is nanotube diameter. The data was divided into two groups to get how the data size allotted for testing and training exaggerated the estimate. 70% of the data were utilized for training and 30% utilized for testing in the suggested ANN model. System parameters of the proposed ANN and SVM models are given in Table 1.

In this study, an ANN model with 1 and 2 hidden layers (HL) is utilized to demonstrate how the amount of HL influences the R^2 and RMSE outcomes. Fig. 4 depicts the entities and flow diagram for the production, simulation, and prediction of TiO_2 nanotubes using ANN and SVM models.

2.4. Analytical model

An analytical model alternative to the simulation model is also proposed for the nanotube diameter using some of numeric analysis methods. If a system of equations consisting of a certain number of unknowns and a certain number of equations consists of linear or nonlinear terms, this system is called a system of linear or nonlinear equations. The proposed system of equations is a linear system containing three unknowns which are voltage, anodization time and NH_4F concentration. If we consider values of these unknowns and tube diameter as a matrix form such as $A.\vec{x} = b$. Where A is parameter of

Table 2
Experimental, analytical and simulation results of nanotube diameter under different anodization voltage, time and electrolyte composition.

Volt (V)	Time (min)	wt	Experimental Results of Nanotube Diameters (nm)	Analytical Results of Nanotube Diameters (nm)	Simulation Results of Nanotube Diameters (nm)			
					Linear SVM	Quadratic SVM	2HL ANN	1HL ANN
20	60	0.5	69.69	67.01175	57.35	67.29	70.39	74.52
20	120	0.5	71.79	75.75375	67.23	83.12	72.18	77.18
20	240	0.5	83.33	93.23775	86.88	88.95	144.05	87.12
30	60	0.5	77.55	96.91275	91.38	90.59	76.74	83.60
30	120	0.5	106.25	105.6548	98.66	108.20	86.64	90.58
30	240	0.5	108.69	123.1388	121.30	110.97	150.22	113.09
40	60	0.5	111.11	126.8138	119.17	116.46	105.91	105.68
40	120	0.5	155.55	135.5558	129.81	129.16	135.42	119.81
40	240	0.5	160	153.0398	146.86	136.88	154.24	154.06
50	60	0.5	150	156.7148	150.80	138.26	136.18	144.32
50	120	0.5	166.66	165.4568	158.90	160.45	193.48	161.90
50	240	0.5	171.42	182.9408	180.47	179.26	165.38	191.58
60	60	0.5	176	186.6158	182.32	177.37	171.33	184.53
60	120	0.5	188.23	195.3578	190.22	200.66	212.96	196.67
60	240	0.5	211.76	212.8418	207.70	211.99	207.54	212.26
70	**60**	**0.5**			**212.15**	**235.64**	**215.04**	**208.99**
70	**120**	**0.5**			**220.65**	**254.73**	**220.85**	**210.52**
70	**240**	**0.5**			**237.66**	**276.60**	**225.57**	**220.60**
20	60	1	72.22	65.4795	56.82	48.54	72.14	75.18
20	120	1	75	74.2215	71.75	77.22	75.37	78.20
20	240	1	94.11	91.7055	90.79	72.93	99.97	89.31
30	60	1	80	95.3805	91.30	89.96	94.25	85.39
30	120	1	95.23	104.1225	99.98	103.36	92.91	93.13
30	240	1	105.96	121.6065	121.24	116.83	103.81	117.41
40	60	1	120	125.2815	121.42	110.95	118.26	109.53
40	120	1	131.64	134.0235	133.40	131.11	138.08	124.48
40	240	1	142.85	151.5075	152.67	146.59	131.44	159.20
50	60	1	133.33	155.1825	156.28	155.63	138.04	149.54
50	120	1	200	163.9245	164.72	166.61	180.35	166.86
50	240	1	211.76	181.4085	181.65	184.40	198.20	194.97
60	60	1	186	185.0835	180.15	170.77	171.18	188.41
60	120	1	215.38	193.8255	189.21	192.83	206.53	199.65
60	240	1	225	211.3095	214.42	230.13	214.53	213.74
70	**60**	**1**			**213.78**	**220.97**	**227.20**	**227.82**
70	**120**	**1**			**222.29**	**239.41**	**233.47**	**230.71**
70	**240**	**1**			**239.29**	**259.99**	**238.87**	**231.14**

unknowns and b is nanotube diameter. After applying one of iterative linear algebra methods which is Jacobi, a mathematical equation which depends on voltage (x_1), anodization time (x_2) and NH_4F concentration (x_3) can be derived as given below.

$$\text{Nanotube Diameter} = 2.9901x_1 + 0.1457x_2 - 3.0645x_3 \quad (9)$$

3. Results and discussion

XRD measurements were used to inspect the outcome of annealing temperature on TiO_2 nanotubes crystalline structure formation. Fig. 5 illustrates the XRD designs of TiO_2 nanotubes annealed and as-prepared at 300 and 700 °C. Before annealing, TiO_2 nanotubes arrays are always amorphous and unsuitable for any application, including electron transport [52–54]. Even though the rutile phase is more chemically consistent than the anatase phase, it is less efficient in sensor implementation [55,56]. Because of its greater refraction index and enhanced particle mobility in the anatase lattice, it possesses better photocatalytic characteristics than rutile [57,58]. As-prepared TiO_2 nanotubes arrays are generally converted to anatase phase by high heat treatment. As a result, as- prepared TiO_2 nanotubes arrays were heated at 300 and 700 °C for 3 h in a dry air environment for crystallization. In the X-ray diffraction patterns of amorphous materials (green lines), the four strongest recognizable peaks that can be attributed to titanium planes are shown: (100), (002), (101), and (102). (102). (102) [59]. At all annealed temperatures (300–700 °C), Pure titanium is still present in the samples; however, the peaks intersect with the whole of the anatase phase. The magnitude of titanium peaks was diminished when the full TiO_2 was converted to rutile. Following a heat treatment at 300 °C, the phase of anatase is visible, with a modest intensity peak at 2θ is about 25 °C. Because anatase is a metastable phase, it changes irreversibly into rutile at temperatures exceeding 700 °C. When the temperature rises, the anatase diffraction peaks eventually fade away and disappear, allowing the rutile phase diffraction patterns to take over [60]. Because transformation to the rutile phase occurs at a greater temperature, this indicates that the anatase phase is the favored growth orientation for TiO_2 nanotubes.

The parameters of the anodization like as anodizing voltage, temperature, time, and electrolyte composition influence the morphology and structure of nanotubes [60]. Many studies have found that the diameter of nanotubes is highly sensitive to changes in anodization voltage [53,58]. SEM pictures of TiO_2 nanotubes anodized at 20 V, 40 V, and 60 V are shown in Fig. 6. It shows the SEM pictures of arranged TiO_2 nanotubes samples on Ti acquired by anodization in glycerol based electrolytes with 0.5% and 1% wt NH_4F by applying anodization potential of 20 V, 40 V and 60 V at 20 °C for 60 min. The cross-section SEM image of the TiO_2 nanotube anodized at 40 V for 240 min is given (Fig. 6). The diameter of TiO_2 nanotubes rises as the anodization voltage increases. The diameter of TiO_2 nanotubes rises as the anodization voltage increases. The diameter of TiO_2 nanotubes increased approximately linearly when the anodization voltage was increased. SEM images were used to measure the nanotube diameters. Since nanotube growth was performed throughout a significantly more comprehensive (F^-) concentration range, it's vital to relate the electrochemical data acquired during anodization in different electrolytes. Fluorides in the electrolyte have a clear effect on the magnitude of the current, which

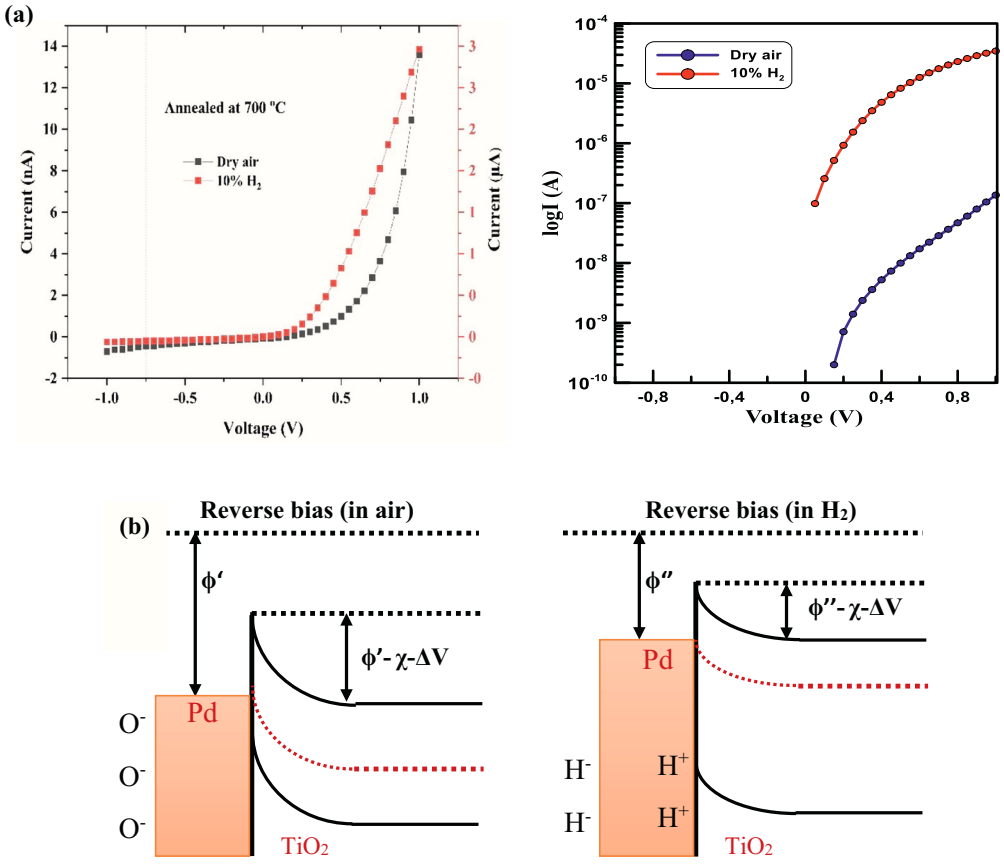

Fig. 7. **(a)** The I-V characteristic of the TiO_2 nanotubes sensors under dry air and 10% H_2 conditions for annealed at 700 °C, **(b)** H_2 sensing mechanism based on the height of the SBH at the interface between Pd and TiO_2 nanotubes.

follows the same pattern as the thickness. The results show that the formation of nanotubes is highly dependent on the concentration of NH_4F [61]. As it clearly seen, anodization voltage and electrolyte concentration are significantly affected the diameters of TiO_2 nanotubes. The diameter of nanotubes can be increased by adjusting the applied voltage. Nanotube size varies greatly contingent on the type of electrolyte, particularly its density. The nanotubes have filled the whole region of the samples and the average diameter of the nanotubes is changing from 70 to 225 nm as seen in Table 2. All the anodization properties are given and the TiO_2 nanotube diameters are measured according to the SEM images. Same magnification images are given to show the difference between the diameters of the nanotubes.

The thermionic emission (TE) method is used to examine the linear part of logarithmic I-V graphs at low voltages and is follows [62]:

$$I = I_0\left[exp\left(\frac{qV}{nkT} - 1\right)\right] \tag{10}$$

Here q is the electron charge, k is the Boltzmann constant, T is the temperature, n is the ideality factor ($n = 1$ for ideal devices), and I_0 is the reverse saturation current:

$$I_0 = AA^*T^2exp\left(\frac{q\varnothing_b}{kT} - 1\right) \tag{11}$$

Here A is the device area, A* is the Richardson constant and Φ_b is the effective Schottky barrier height (SBH). The SBH equation according to TE is as follows:

$$\varnothing_b = \frac{kT}{q}ln\left(\frac{AA^*T^2}{I_0}\right) \tag{12}$$

The current of sensor devices was measured with applying voltage sweep between 1 to −1 V to see the effect of crystal structure (amorphous, anatase and rutile). As previously observed, the fluctuation in the I–V curve caused by H_2 was normal for a Schottky diode-type sensor [63]. The electron transport from TiO_2 to Pd established the SBH at the interface between Pd and TiO_2 nanotubes, resulting in the establishment of a depletion area. The barrier height on the Pd side remains constant while the bias voltage is changed, whereas the barrier height on the TiO_2 side and the width of the exhausted layer rise under reverse bias. Environmental oxygen adsorbs on the surfaces of TiO_2 nanotubes and Pd, absorbs electrons from the material, and ionizes to O^- or O^{2-}. When a reducing gas like H_2 reacts with adsorbed oxygen, electrons are pumped back into the conduction band, lowering the barrier height [64]. As a result, raising the applied reverse bias could improve gas sensitivity since a higher barrier height could result in a larger drop in sensing resistance. However, even in 10% H_2, a non-linear I–V curve was found, indicating the presence of a SBH at the interface between Pd and TiO_2, while the barrier height was significantly reduced in 10% H_2 balanced with air compared to dry air for annealed at 700 °C nanotubes as given in Fig. 7a and b. The I-V characteristic of unannealed and annealed at 300 °C TiO_2 also displayed Schottky-type behavior.

In order to elucidate concentration depending on H_2 gas sensing behavior, 0.05 V is applied to Pd/TiO_2 nanotubes/ Ti sensor device structure and the current is measured continuously by changing the atmospheric condition of the measurement cell. Fig. 8a shows the current of TiO_2 nanotubes annealed at 300 °C as a function of time by enhancing H_2 concentration from 0.5% to 10%. After the nanotube device exposed to 0.5% H_2, the current of the device is sharply increased and then come to saturation value from 1.02 μA to 0.83 mA. Subsequently, while the other indicated concentration (1, 2, 5 and 10%) of H_2 exposed to measurement cell, similarly the current of the device

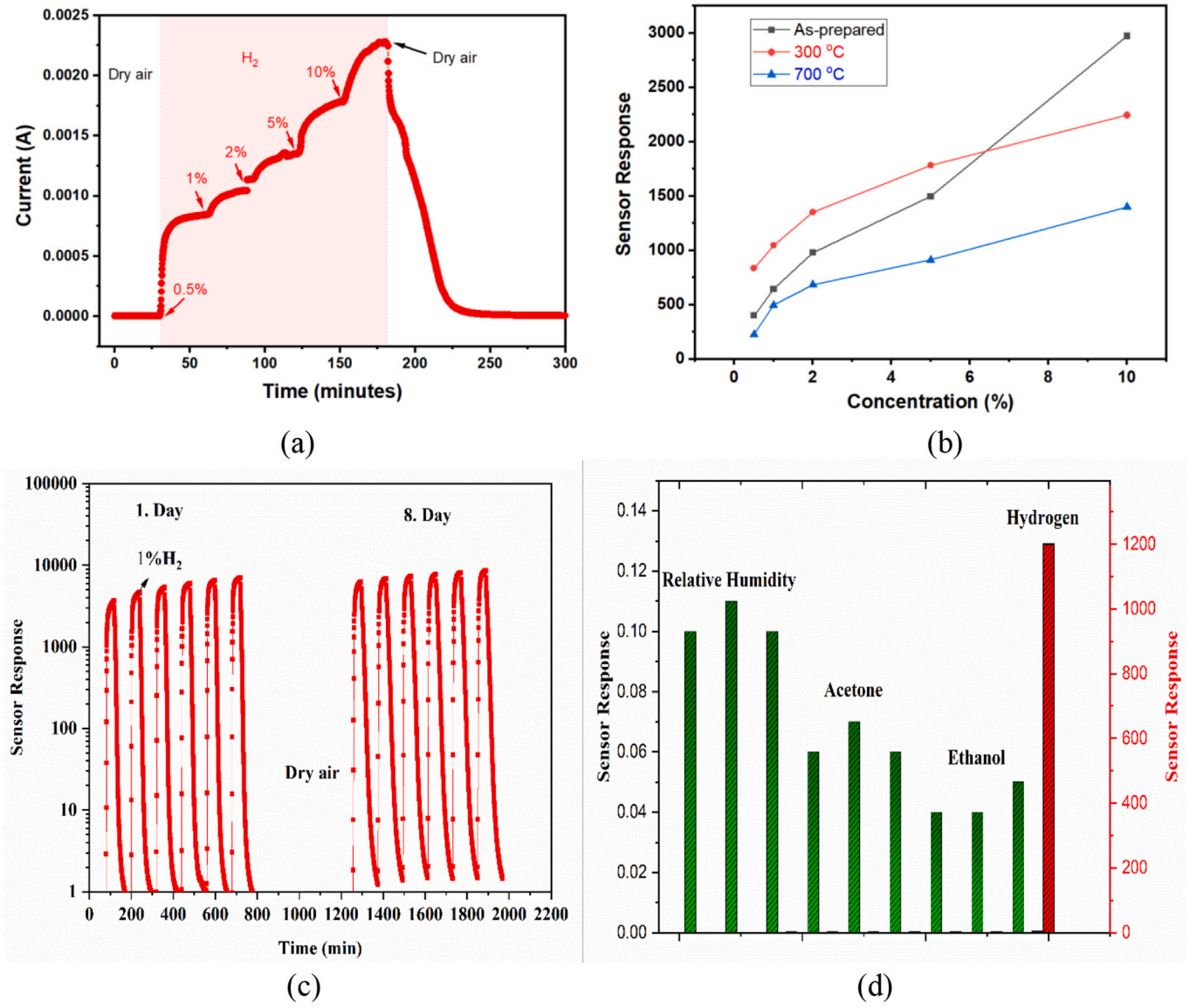

Fig. 8. (a) The current versus time for TiO_2 nanotubes annealed at 300 °C by exposing different concentrations of H_2 and (b) sensor response as a function of concentration for all sensor devices at room temperature (c) long-term sensitivity as a function of time (d) sensor response for the different gas.

increased sharply and then came to saturation. The increase in the current by exposure to H_2 could be explained with the decrease of the barrier height between TiO_2 and Pd. During cleaning the measurement cell with dry air, the current of the nanotubes decreased and came to baseline value as seen in Fig. 8a. Sensor response could be defined as;

$$\text{Sensor Response (R)} = \frac{\Delta I}{I_A} = \frac{I_H - I_A}{I_A} \tag{13}$$

where I_H is the current after the sensor is exposed to H_2, and I_A is the baseline value of the sensor exposed to dry air. The sensor responses of as-prepared, annnealed at 300 °C and 700 °C are increased with increasing H_2 concentration as given in Fig. 8b. The highest sensor response is observed for anatase TiO_2 nanotubes that annealed at 300 °C except for 10% H_2 concentration. Previously, anatase TiO_2 nanotubes that synthesized with anodization method from Ti thin film showed the best sensitivity for volatile organic compound (VOC) sensing [65]. The concentration of 1% H_2 gas exposed to the sensor device that annealed at 300 °C and the sensor response has no significant change for long-term sensitivity as a result of eight-day measurement as shown in Fig. 8c. In order to determine the selectivity of the TiO_2 nanotubes device that annealed at 300 °C, the device are tested for the relative humidity, ethanol and acetone sensing. The concentration of the relative humidity, ethanol and acetone are 50%, 1% and 2%, respectively at room temperature. The sensor response of is around 0.1 which can be negligibly small compare to the 1% H_2 exposure as shown in Fig. 8d. Therefore, these results shows that nanotubes device is not sensitive to the humidity, ethanol and acetone.

Anodic oxidation is a simple and efficient method for creating highly ordered, tube-shaped porous TiO_2 arrays at the nanoscale. Furthermore, anodization parameters such as anodization time, voltage and concentration can be used to modify the morphology of TiO_2 nanotubes such as nanotube diameter, thickness, and length. Sreekantan et al. reported that the anodization voltage really plays a significant role in determining the homogeneity and uniformity of the size distribution of the nanotube in their study using an anodization voltage between 5 V and 30 V. They emphasized that as the anodization voltage increased, the two tubes combined to form a single tube, thus changing the tube radius and homogeneity [66]. In this study, it is seen that the tube radii are homogeneous and in a single form at low anodization voltage up to 40 V. However, as the applied voltage increases, it is seen that the tubes

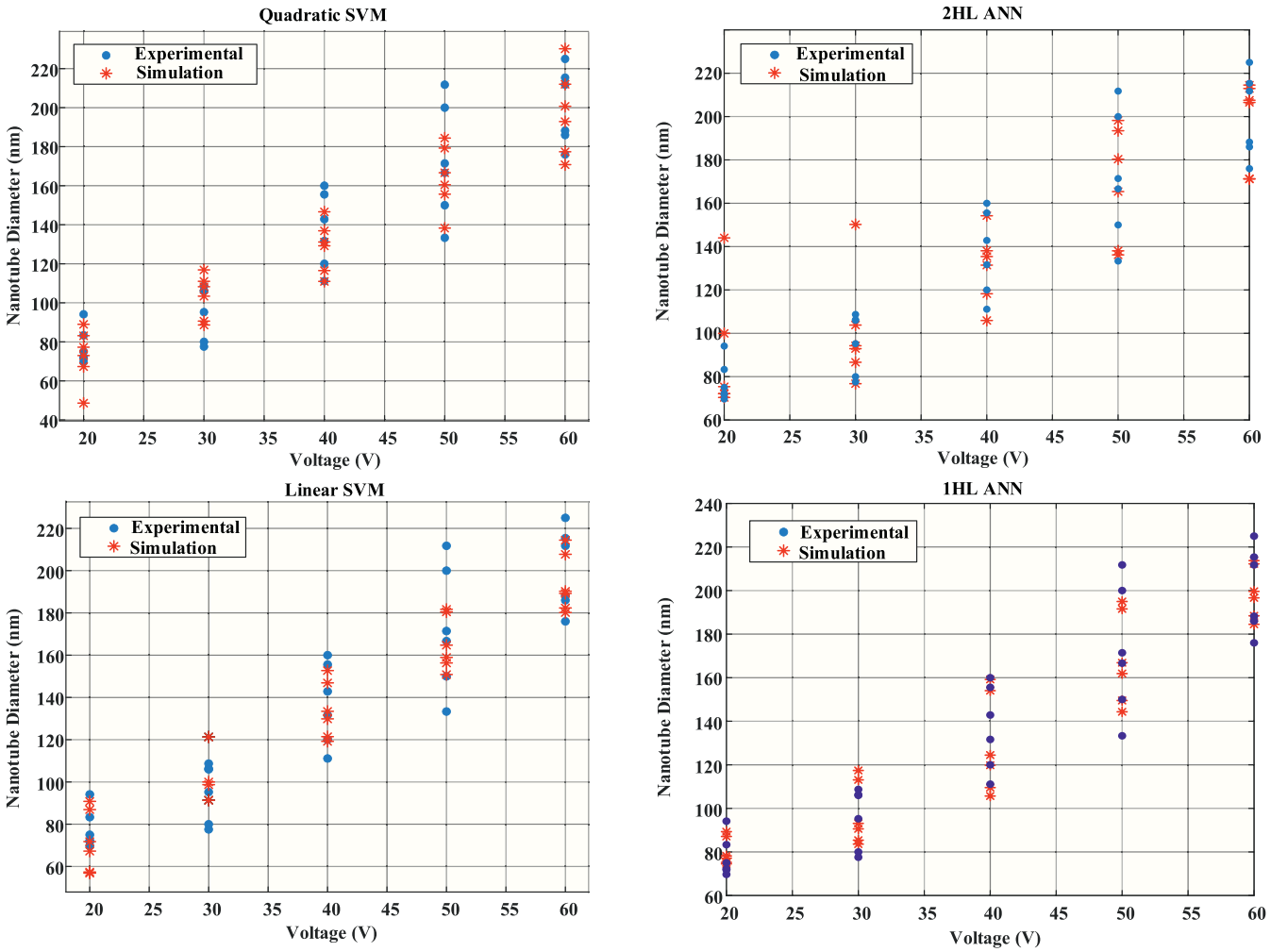

Fig. 9. Experimental and simulation results of nanotube diameter versus voltage.

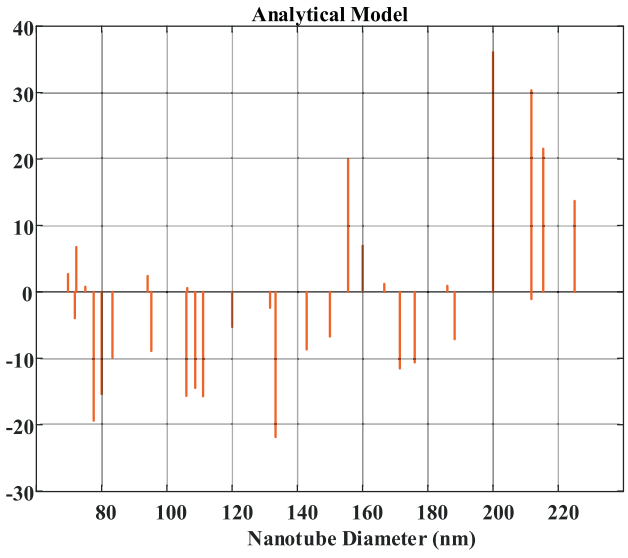

Fig. 10. Residuals between analytical and experimental results of nanotube diameter.

coalesce and their diameters vary between 50 and 200 nm. Thus, it is seen that the anodization voltage changes tube homogeneity and uniformity at high anodization voltage. And also, numerous studies show that nanotube diameters are quite sensitive to changing anodization conditions [67]. Therefore these parameters are used to simulate and prediction of nanotubes diameters. Thirty different TiO_2 nanotubes were fabricated and their detailed anodization properties were given in Table 2. It is clearly seen that the average diameters of the produced TiO_2 nanotubes increase depending on the anodization voltage and time. In fact, increasing the NH_4F ratio of the electrolyte generally resulted in an increase in the average TiO_2 nanotubes diameters. Linear SVM, Quadratic SVM, 1HL ANN and 2HL ANN models are used for the simulation and prediction process of the nanotube diameter data of experimental samples. The simulation and prediction results of nanotube diameters obtained from the proposed models for different anodization voltage, time and electrolyte composition comparatively. The anodization voltage of 70 V was not obtained experimentally for both 0.5% and 1% electrolyte compositions. Therefore, the TiO_2 nanotubes diameter at 70 V anodization voltage were predicted using ANN and SVM models and analytical results by using Eq. (9) are also given in Table 2.

Nanotube diameter versus voltage graphs are given in Fig. 9 for the proposed SVM and ANN models to show how the experimental and simulation results close to each other with different colors and symbols to increase visibility. As given in the figure, simulation and experimental outcomes are coincided more with using of the 1HL ANN model.

Residual plot is also shown in Fig. 10 for analytical model and Fig. 11 for ANN and SVM models to show errors between experimental, analytical and simulation data. As shown from the residual plots, although residual values are obtained between ±30 for analytical

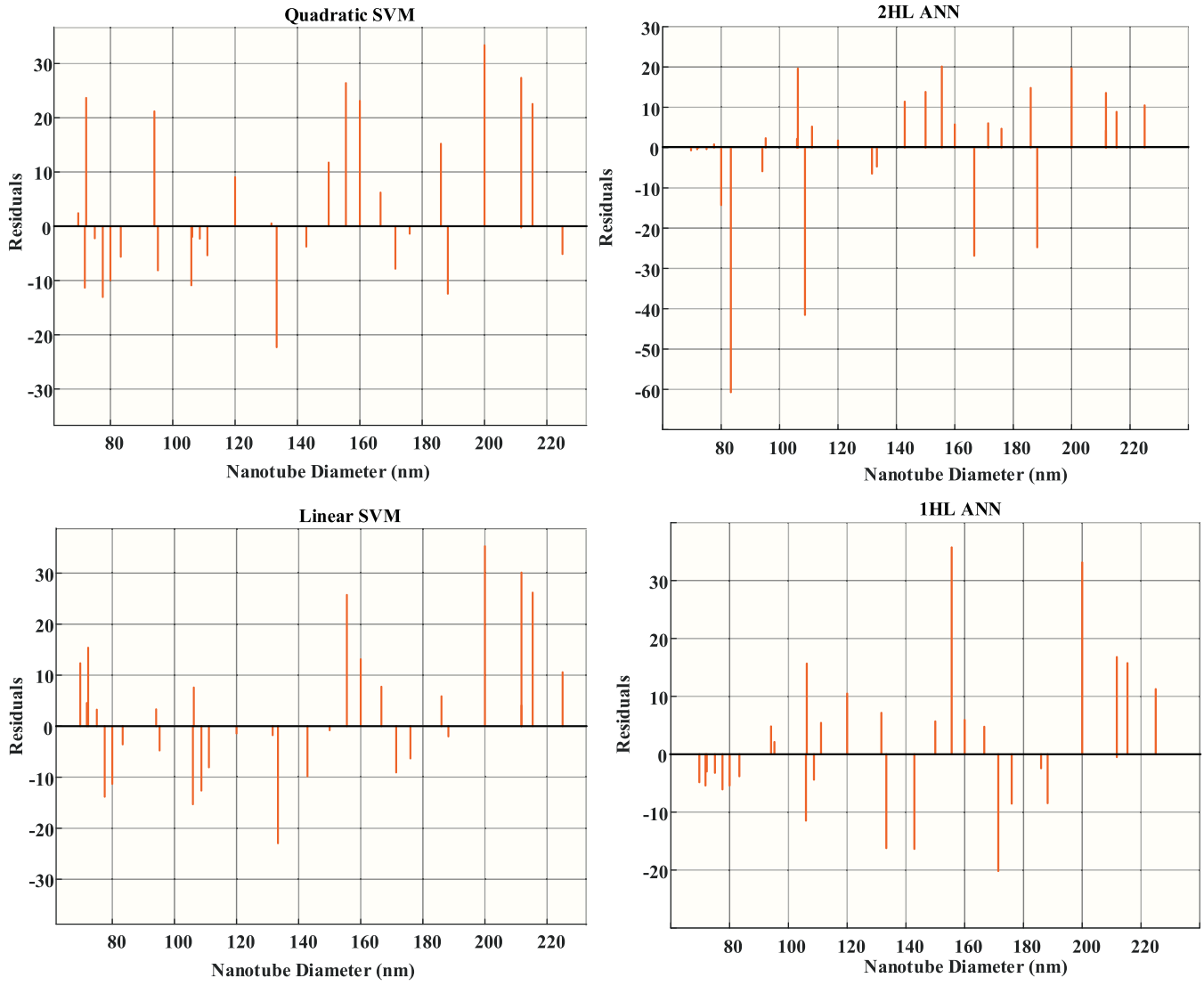

Fig. 11. Residuals between experimental and simulation results of nanotube diameter.

Table 3
RMSE and R^2 values for ANN and SVM models.

Model	Linear-SVM	Quadratic-SVM	2HL-ANN	1HL-ANN
RMSE	14.082	14.741	15.247	11.816
R^2	0.93	0.92	0.93	0.96

model, linear SVM, quadratic SVM and 2HL ANN, it is obtained between +30 and − 20 for the 1HL ANN model.

RMSE and R^2 values are also obtained for all SVM and ANN models to show which model is the best to simulate and predict experimental data in the future. These rates are donated in Table 3 relatively. The amount of RMSE and determination are predictable to turn out to be around 1 and 0 consistently. The best and worst R^2 values are obtained as 0.96 for 1HL ANN and 0.92 for the Quadratic SVM model for testing and training outcomes of the model. The best and worst RMSE values are 11.816 for 1HL ANN and 15.247 for the 2HL ANN model.

4. Conclusions

In conclusion, TiO_2 nanotubes with inner diameters ranging from 70 to 225 nm were effectively produced on titanium foil using anodic oxidation, and the effect of the crystal structure on the H_2 sensing characteristics of TiO_2 nanotubes-based sensors were examined. Unannealed and annealed TiO_2 nanotubes displayed a typical Schottky-type behavior from I-V measurement under dry air condition and exposed to 10% H_2. At ambient temperature, the hydrogen sensing characteristics of TiO_2 nanotubes in the form of a Ti/TiO_2 nanotubes/Pd device were investigated with concertation ranging from 0.5 to 10% depending on the crystalline phase. Anatase crystalline TiO_2 nanotubes have the maximum sensor response. We also afforded to objective methodologies for designing better simulation and prediction for nanotube diameter applications. For this purpose, the nanotube diameter is analyzed and predicted from voltage, time and electrolyte composition by using the proposed analytical and simulation models. All of the simulation, analytical and experimental results are compared and a very high similarity is obtained for the simulation based 1HL ANN model. The similarity between results is shown with residual and RMSE values. These results show us that the proposed models can be used for the prediction of nanotube diameters without doing any further experiments.

Research data policy and data availability statements

Data sharing not applicable to this article as no datasets were generated or analyzed during the current study.

Sample credit author statement

The review and preparation of the manuscript were done by **Esme Isik, L. Bilal Tasyurek, Ibrahim Isik, and Necmettin Kilinc.** The data analysis and final revision of the paper, as well as the preparation of figures, were done by all of the authors. The findings and interpretation were agreed upon by all of the writers after they had read the text.

Funding

This study was funded by Inonu University Scientific Research Unit of Turkey (BAP, Project Number: FBA-2020-2315).

Declaration of Competing Interest

The authors declare the following financial interests/personal relationships which may be considered as potential competing interests:

Ibrahim ISIK reports financial support was provided by Inonu University.

References

[1] J.O. Abe, A.P.I. Popoola, E. Ajenifuja, O.M. Popoola, Hydrogen energy, economy and storage: review and recommendation, Int. J. Hydrog. Energy 44 (29) (2019) 15072–15086, https://doi.org/10.1016/j.ijhydene.2019.04.068.

[2] Y. Wang, M. Yang, G. Zhang, J. Dai, Y. Zhang, Z. Zhuang, Ultra-highly sensitive hydrogen sensor based on fiber Fabry-Perot interferometer with Pt/WO3 coating, in: 23rd International Conference on Optical Fibre Sensors vol. 9157, 2014, p. 91574F.

[3] B. Wu, C. Zhao, B. Xu, Y. Li, Optical fiber hydrogen sensor with single Sagnac interferometer loop based on Vernier effect, Sensors Actuators B Chem. 255 (2018) 3011–3016, https://doi.org/10.1016/j.snb.2017.09.124.

[4] T. Hübert, L. Boon-Brett, G. Black, U. Banach, Hydrogen sensors–a review, Sensors Actuators B Chem. 157 (2) (2011) 329–352.

[5] R. Zazpe, et al., Laboratory of Nanostructures and Nanomaterials, Institute of Physics of the CAS, v.v.i., Na Slovance 2, 182 21 Prague 8, 2017, https://doi.org/10.1021/acs.langmuir.7b00187.

[6] J. Chen, et al., Photo-functionalized TiO2 nanotubes decorated with multifunctional ag nanoparticles for enhanced vascular biocompatibility, Bioact. Mater. 6 (1) (Jan. 2021) 45–54, https://doi.org/10.1016/J.BIOACTMAT.2020.07.009.

[7] Z. Lin, et al., The conduction process of grain and grain boundary in the semiconductive zirconium oxynitride thin film, Semicond. Sci. Technol. 34 (8) (2019), https://doi.org/10.1088/1361-6641/ab2c0e.

[8] N. Kilinç, E. Şennik, D. Atilla, A.G. Gürek, V. Ahsen, Z.Z. Öztürk, Effect of ambient atmosphere on photoconductivity of TiO2 nanotube-CupC heterojunction, Sci. Adv. Mater. 5 (4) (2013) 373–379, https://doi.org/10.1166/sam.2013.1467.

[9] K.M. Chahrour, F.K. Yam, R. Abdalrheem, High-performance UV photodetector of anodic rutile TiO2 nanotube arrays, Mater. Lett. 248 (Aug. 2019) 161–164, https://doi.org/10.1016/J.MATLET.2019.04.029.

[10] W. Wei, M. Valvo, K. Edströ, and L. Nyholm, "Size-Dependent Electrochemical Performance of Monolithic Anatase TiO 2 Nanotube Anodes for Sodium-Ion Batteries," doi: https://doi.org/10.1002/celc.201701267.

[11] L.K. Preethi, T. Mathews, M. Nand, S.N. Jha, C.S. Gopinath, S. Dash, Band alignment and charge transfer pathway in three phase anatase-rutile-brookite TiO2 nanotubes: an efficient photocatalyst for water splitting, Appl. Catal. B Environ. 218 (Dec. 2017) 9–19, https://doi.org/10.1016/J.APCATB.2017.06.033.

[12] P.-Y. Hsieh, Y.-H. Chiu, T.-H. Lai, M.-J. Fang, Y.-T. Wang, Y.-J. Hsu, TiO 2 Nanowire-Supported Sulfide Hybrid Photocatalysts for Durable Solar Hydrogen Production, 2018, https://doi.org/10.1021/acsami.8b17858.

[13] J. Guo, et al., One-step synthesis of mesoporous TiO2 film for high photon-to-electron transport efficiency in dye-sensitized solar cells, J. Alloys Compd. 770 (2019) 662–668, https://doi.org/10.1016/j.jallcom.2018.08.175.

[14] S. Lin, D. Li, J. Wu, X. Li, S.A. Akbar, A selective room temperature formaldehyde gas sensor using TiO2 nanotube arrays, Sensors Actuators B Chem. 156 (2) (Aug. 2011) 505–509, https://doi.org/10.1016/J.SNB.2011.02.046.

[15] D. Gong, et al., Titanium oxide nanotube arrays prepared by anodic oxidation, J. Mater. Res. 16 (12) (2001) 3331–3334, https://doi.org/10.1557/JMR.2001.0457.

[16] W. Guo, X. Xue, S. Wang, C. Lin, Z.L. Wang, An integrated power pack of dye-sensitized solar cell and Li battery based on double-sided TiO2 nanotube arrays, Nano Lett. 12 (5) (2012) 2520–2523.

[17] J. Guo, et al., One-step fabrication of TiO2/graphene hybrid mesoporous film with enhanced photocatalytic activity and photovoltaic performance, Chin. J. Catal. 41 (8) (2020) 1208–1216, https://doi.org/10.1016/S1872-2067(19)63511-4.

[18] N.K. Allam, C.A. Grimes, Effect of cathode material on the morphology and photoelectrochemical properties of vertically oriented TiO2 nanotube arrays, Sol. Energy Mater. Sol. Cells 92 (11) (2008) 1468–1475.

[19] Y. Zhang, et al., Synthesis and characterization of TiO2 nanotubes for humidity sensing, Appl. Surf. Sci. 254 (17) (2008) 5545–5547.

[20] L. Li, C. Xie, X. Xiao, Polydopamine modified TiO2 nanotube arrays as a local drug delivery system for ibuprofen, J. Drug Deliv. Sci. Technol. 56 (2020) 101537.

[21] A.V. Lashkov, et al., The Ti wire functionalized with inherent TiO2 nanotubes by anodization as one-electrode gas sensor: a proof-of-concept study, Sensors Actuators B Chem. 306 (2020) 127615.

[22] C.A. Grimes, Synthesis and application of highly ordered arrays of TiO 2 nanotubes, J. Mater. Chem. 17 (15) (2007) 1451–1457.

[23] H.F. Lu, et al., Amorphous TiO2 nanotube arrays for low-temperature oxygen sensors, Nanotechnology 19 (40) (2008) 405504.

[24] M. Y. P, M.A.V. Zwilling, A. Boutry-Forveille Darque-Ceretti, D. David, Structure and growth of anodic oxide films on titanium and TA6V alloy, Surf. Interface Anal. 27 (2) (1999) 629–637, https://doi.org/10.1016/0022-5088(77)90043-1.

[25] R. Beranek, H. Hildebrand, P. Schmuki, Self-organized porous titanium oxide prepared in H2SO4/HF electrolytes, Electrochem. Solid-State Lett. 6 (3) (2003) 23–25, https://doi.org/10.1149/1.1545192.

[26] M. Paulose, O.K. Varghese, G.K. Mor, C.A. Grimes, K.G. Ong, Unprecedented ultra-high hydrogen gas sensitivity in undoped titania nanotubes, Nanotechnology 17 (2) (2006) 398–402, https://doi.org/10.1088/0957-4484/17/2/009.

[27] O.K. Varghese, D. Gong, M. Paulose, K.G. Ong, C.A. Grimes, Hydrogen sensing using titania nanotubes, Sensors Actuators B Chem. 93 (1–3) (2003) 338–344, https://doi.org/10.1016/S0925-4005(03)00222-3.

[28] E. Şennik, Z. Çolak, N. Kilinç, Z.Z. Öztürk, Synthesis of highly-ordered TiO2 nanotubes for a hydrogen sensor, Int. J. Hydrog. Energy 35 (9) (2010) 4420–4427, https://doi.org/10.1016/j.ijhydene.2010.01.100.

[29] Y. Ge, W. Zhu, X. Liu, S. Liu, Electrochemical fabrication of titania nanotube arrays with tunning nature of dimethyl sulfoxide and its application for hydrogen sensing, J. Nanosci. Nanotechnol. 12 (4) (2012) 3026–3034.

[30] H. Liu, D. Ding, C. Ning, Z. Li, Wide-range hydrogen sensing with Nb-doped TiO2 nanotubes, Nanotechnology 23 (1) (2011) 15502.

[31] Z. Chen, J.J. Wang, Y. Ren, C. Yu, K. Shum, Schottky solar cells based on CsSnI3 thin-films, Appl. Phys. Lett. 101 (9) (2012) 93901.

[32] Z. Li, D. Ding, Q. Liu, C. Ning, Hydrogen sensing with Ni-doped TiO2 nanotubes, Sensors 13 (7) (2013) 8393–8402.

[33] J. Lee, D.H. Kim, S.-H. Hong, J.Y. Jho, A hydrogen gas sensor employing vertically aligned TiO2 nanotube arrays prepared by template-assisted method, Sensors Actuators B Chem. 160 (1) (2011) 1494–1498, https://doi.org/10.1016/j.snb.2011.08.001.

[34] C.-H. Han, D.-W. Hong, I.-J. Kim, J. Gwak, S.-D. Han, K.C. Singh, Synthesis of Pd or Pt/titanate nanotube and its application to catalytic type hydrogen gas sensor, Sensors Actuators B Chem. 128 (1) (2007) 320–325, https://doi.org/10.1016/j.snb.2007.06.025.

[35] H. Xun, Z. Zhang, A. Yu, J. Yi, Remarkably enhanced hydrogen sensing of highly-ordered SnO2-decorated TiO2 nanotubes, Sensors Actuators B Chem. 273 (2018) 983–990, https://doi.org/10.1016/j.snb.2018.06.120.

[36] X. Wei, et al., A novel hydrogen-sensitive sensor based on Pd nanorings/TNTs composite structure, Int. J. Hydrog. Energy 42 (38) (2017) 24580–24586, https://doi.org/10.1016/j.ijhydene.2017.07.167.

[37] M.H. Ahmadi, B. Mohseni-Gharyehsafa, M. Farzaneh-Gord, R.D. Jilte, R. Kumar, K. Wing Chau, Applicability of connectionist methods to predict dynamic viscosity of silver/water nanofluid by using ANN-MLP, MARS and MPR algorithms, Eng. Appl. Comput. Fluid Mech. 13 (1) (2019) 220–228, https://doi.org/10.1080/19942060.2019.1571442.

[38] H. Zhang, J. Zhao, Y. Jia, X. Xu, C. Tang, Y. Li, Exploration of artificial neural network to predict morphology of TiO 2 nanotube, Expert Syst. Appl. 39 (4) (2012) 4094–4101, https://doi.org/10.1016/j.eswa.2011.09.081.

[39] S. Wang, et al., Machine-learning micropattern manufacturing, Nano Today 38 (2021) 101152, https://doi.org/10.1016/j.nantod.2021.101152.

[40] N. Kilinc, Palladium and platinum thin films for low-concentration resistive hydrogen sensor: a comparative study, J. Mater. Sci. Mater. Electron. 32 (5) (2021) 5567–5578, https://doi.org/10.1007/s10854-021-05279-w.

[41] Support Vector Machines, *SpringerReference*, Springer-Verlag, 1992. Boser, Guyon, Vapnik.

[42] A. Widodo, B.-S. Yang, Support vector machine in machine condition monitoring and fault diagnosis, Mech. Syst. Signal Process. 21 (6) (2007) 2560–2574, https://doi.org/10.1016/j.ymssp.2006.12.007.

[43] E. Kabir, Siuly, Y. Zhang, Epileptic seizure detection from EEG signals using logistic model trees, Brain Inform. 3 (2) (2016) 93–100, https://doi.org/10.1007/s40708-015-0030-2.

[44] B. Schölkopf, A.J. Smola, Smola, A.: Learning with Kernels - Support Vector Machines, Regularization, Optimization and Beyond vol. 98, MIT Press, Cambridge, MA, 2001.

[45] I. Isik, E. Isik, H. Toktamis, Dose and fading time estimation of glass ceramic by using artificial neural network method, DÜMF Mühendislik Derg 12 (1) (2020) 47–52, https://doi.org/10.24012/dumf.703171.

[46] Y. Bayraktar, A. Özyılmaz, M. Toprak, E. Işık, F. Büyükakın, M.F. Olgun, Role of the health system in combating Covid-19: cross-section analysis and artificial neural network simulation for 124 country cases, Soc. Work Public Health 00 (00) (2020) 1–16, https://doi.org/10.1080/19371918.2020.1856750.

[47] M.C. Demet Demir Sahin, Esme Isik, Ibrahim Isik, Artificial neural network modeling for the effect of fly ash fineness on compressive strength, Arab. J. Geosci. 14 (2705) (2021).

[48] E. Isik, D. Toktamis, M. Bilal Er, M. Hatib, Classification of Thermoluminescence Features of CaCO 3 with Long Short-Term Memory Model, 2021, https://doi.org/10.1002/bio.4109.

[49] E. Isik, Analyzing of the diffusion constant on the nano-scale systems by using artificial neural networks, AIP Adv. 11 (10) (Oct. 2021), https://doi.org/10.1063/5.0067795.
[50] S.M.J. Pappu, S.N. Gummadi, Artificial neural network and regression coupled genetic algorithm to optimize parameters for enhanced xylitol production by Debaryomyces nepalensis in bioreactor, Biochem. Eng. J. 120 (2017) 136–145, https://doi.org/10.1016/j.bej.2017.01.010.
[51] Q. Yang, S. Le Blond, R. Aggarwal, Y. Wang, J. Li, New ANN method for multi-terminal HVDC protection relaying, Electr. Power Syst. Res. 148 (2017) 192–201, https://doi.org/10.1016/j.epsr.2017.03.024.
[52] Y. Alivov, P. Xuan, Z.Y. Fan, TiO 2 Nanotube Height Effect on the Efficiency of Dye-Sensitized Solar Cells, 2011, https://doi.org/10.1007/s11051-011-0627-1.
[53] T. Hoseinzadeh, Z Ghorannevis, M Ghoranneviss, A H Sari, and M K Salem, "Effects of Various Applied Voltages on Physical Properties of TiO 2 Nanotubes by Anodization Method," doi: https://doi.org/10.1007/s40094-017-0257-9.
[54] Y. Alivov, M. Pandikunta, S. Nikishin, Z.Y. Fan, The anodization voltage influence on the properties of TiO2 nanotubes grown by electrochemical oxidation, Nanotechnology 20 (22) (2009), https://doi.org/10.1088/0957-4484/20/22/225602.
[55] X. Li, H. Jin, A. Gaskov, J. Yi, A. Yu, H. Xun, Improving Hydrogen Sensing Performance of TiO 2 Nanotube Arrays by ZnO Modification 6, 2019, p. 70, https://doi.org/10.3389/fmats.2019.00070.
[56] H. Kwon, Y. Lee, S. Hwang, J.K. Kim, Highly-sensitive H2 sensor operating at room temperature using Pt/TiO2 nanoscale Schottky contacts, Sensors Actuators B Chem. 241 (2017) 985–992, https://doi.org/10.1016/j.snb.2016.11.022.
[57] X. Chen, S.S. Mao, Titanium dioxide nanomaterials: synthesis, properties, modifications and applications, Chem. Rev. 107 (7) (2007) 2891–2959, https://doi.org/10.1021/cr0500535.
[58] R. Narayanan, T.Y. Kwon, K.H. Kim, TiO2 nanotubes from stirred glycerol/NH4F electrolyte: roughness, wetting behavior and adhesion for implant applications, Mater. Chem. Phys. 117 (2–3) (2009) 460–464, https://doi.org/10.1016/j.matchemphys.2009.06.023.
[59] M.M. Muzakir, Z. Zainal, H.N. Lim, A.H. Abdullah, N.N. Bahrudin, M.S.M. Ali, Electrochemically reduced titania nanotube synthesized from glycerol-based electrolyte as supercapacitor electrode, Energies 13 (11) (2020), https://doi.org/10.3390/en13112767.
[60] M. Jarosz, et al., Heat treatment effect on crystalline structure and photoelectrochemical properties of anodic TiO2 nanotube arrays formed in ethylene glycol and glycerol based electrolytes, J. Phys. Chem. C 119 (42) (2015) 24182–24191, https://doi.org/10.1021/acs.jpcc.5b08403.
[61] H.I. Jaafar, A.M.A. Alsammerraei, H.H. Hamdan, Study of the effect of NH 4 F concentration on the structure of electrochemically prepared TiO 2 nanotubes المحضرة الكتروكيميائيا TiO 2 عمى تركيب الانابيب النانوية لـ NH 4 F تاثير تركيز 827–831 (2012) (2) 53 رد اسة.
[62] L.B. Taşyürek, Ş. Aydoğan, M. Sevim, Z. Çaldıran, Synthesis of nickel nanoparticles-deposited strontium titanate nanocubes (Ni-STO) and heterojunction electrical applications over a wide temperature range, Mater. Sci. Eng. B 274 (2021) 115479, https://doi.org/10.1016/j.mseb.2021.115479.
[63] T. Iwanaga, T. Hyodo, Y. Shimizu, M. Egashira, H2 sensing properties and mechanism of anodically oxidized TiO2 film contacted with Pd electrode, Sensors Actuators B Chem. 93 (1–3) (2003) 519–525, https://doi.org/10.1016/S0925-4005(03)00181-3.
[64] Y. Ling, F. Ren, J. Feng, Reverse bias voltage dependent hydrogen sensing properties on Au-TiO2 nanotubes Schottky barrier diodes, Int. J. Hydrog. Energy 41 (18) (2016) 7691–7698, https://doi.org/10.1016/j.ijhydene.2016.02.007.
[65] E. Sennik, N. Kilinc, Z.Z. Ozturk, Electrical and VOC sensing properties of anatase and rutile TiO2 nanotubes, J. Alloys Compd. 616 (Dec. 2014) 89–96, https://doi.org/10.1016/J.JALLCOM.2014.07.097.
[66] S. Sreekantan, R. Hazan, Z. Lockman, Photoactivity of anatase–rutile TiO2 nanotubes formed by anodization method, Thin Solid Films 518 (1) (Nov. 2009) 16–21, https://doi.org/10.1016/J.TSF.2009.06.002.
[67] B. Bozkurt Çırak, et al., Synthesis, surface properties, crystal structure and dye sensitized solar cell performance of TiO2 nanotube arrays anodized under different voltages, Vacuum 144 (Oct. 2017) 183–189, https://doi.org/10.1016/J.VACUUM.2017.07.037.